

A MUTAGENETIC TREE HIDDEN MARKOV MODEL FOR LONGITUDINAL CLONAL HIV SEQUENCE DATA

NIKO BEERENWINKEL AND MATHIAS DRTON

ABSTRACT. RNA viruses provide prominent examples of measurably evolving populations. In HIV infection, the development of drug resistance is of particular interest, because precise predictions of the outcome of this evolutionary process are a prerequisite for the rational design of antiretroviral treatment protocols. We present a mutagenetic tree hidden Markov model for the analysis of longitudinal clonal sequence data. Using HIV mutation data from clinical trials, we estimate the order and rate of occurrence of seven amino acid changes that are associated with resistance to the reverse transcriptase inhibitor efavirenz.

1. INTRODUCTION

In the developed world, patients infected with human immunodeficiency virus (HIV) are treated with combinations of several antiretroviral drugs in order to maximally suppress virus replication. However, the development of drug resistant virus variants limits the success of this intervention (Clavel and Hance, 2004). The genetic basis for the emergence of drug resistance is the high mutation rate in HIV, which is a result of the absence of a proof-reading mechanism for reverse transcription of RNA into DNA. The frequent mutations may alter the genetic composition of drug targets and create drug resistant mutants that will outcompete the wild type virus and eventually dominate the intra-host virus population. The applied drug cocktail then becomes ineffective and the patient experiences an increase in virus load.

The accumulation of resistance-conferring mutations is a stochastic process that typically follows one of several co-existing evolutionary pathways (Boucher et al., 1992; Molla et al., 1996; Shafer and Schapiro, 2005). Understanding the pathways to drug resistance is important for the design of effective drug combinations. For the study of these pathways, two types of DNA sequence data, based on either population or clonal sequencing, are available.

In routine clinical diagnostics, viral drug targets are sequenced after therapy failure and prior to a therapy switch. Typically, population sequencing is applied, which results in one DNA sequence that represents the mixture of viruses in the population. This approach detects only those mutations that are present in at least 20% of the strains. Furthermore, the phase information, i.e., the knowledge whether polymorphisms at different sites actually co-occur on the same genome, is lost in population sequencing. Abundant in public databases (Rhee et al., 2003), cross-sectional data obtained from population sequencing have been used to demonstrate correlations between the occurrences of different mutations (Gonzales et al., 2003; Sing et al., 2005). Mutagenetic tree models, a subclass of Bayesian networks based on directed trees (Beerenwinkel et al., 2005b), take such correlation analysis a step further by providing a tool particularly suited to infer evolutionary pathways to drug resistance from cross-sectional data (Beerenwinkel et al., 2005a).

A more elaborate alternative to population sequencing is clonal sequencing. In this approach, multiple viral genomes are independently amplified by PCR and sequenced. This

strategy has two major advantages over population sequencing. First, since mutations may occur in PCR reactions, the use of multiple independent PCR reactions reduces the impact of early and erroneous introduction of mutations at this step of the analysis. Second, in clonal sequencing, the genotype of a single strain is determined. From the resulting haplotypes the linkage between mutations is readily assessed.

While haplotypes provide exact information on the correlation between mutations, we can gain additional insight about the order in which substitutions are fixed into the population from longitudinal data obtained by sequencing viruses from the same patient at multiple time points. In this paper, we propose an extension of the mutagenetic tree model to a model for longitudinal clonal HIV sequence data. The new model captures both the time structure per patient and the clonal variation per time point, and thus allows to employ time structure in the estimation of substitution rates of resistance-conferring mutations. Knowledge of these substitution rates, which can be interpreted as waiting times, provides the basis for rational therapy planning. Indeed, using viral evolutionary information encoded in mutagenetic trees has recently been shown to significantly improve predictions of *in vivo* virological response to antiretroviral combination therapies (Beerenwinkel et al., 2005d).

Rather than modeling viral evolution in full generality, we intend to describe a specific phase of evolution in terms of a specific set of genetic events. More precisely, we model amino acid changes that confer drug resistance under the constant selective pressure of a given drug. The data analyzed in this paper comprise a total of 3350 clones that have been collected from 163 patients at different time points during three phase II clinical studies of the reverse transcriptase (RT) inhibitor efavirenz (Bacheler et al., 2001, 2000). We focus on seven amino acid substitutions in the HIV-1 RT that are associated with resistance to efavirenz (cf. Table 1, where each observed clone is coded as a binary vector of length seven). Working on protease sequences obtained from the same efavirenz studies, Foulkes and DeGruttola (2003) have modeled evolutionary pathways to drug resistance by grouping the observed clones into five clusters and estimating transition rates between clusters. In that approach, however, neither the dependence structure between single mutations nor their rates of occurrence is modelled explicitly. In addition, clonal variation is not incorporated explicitly.

Under treatment with efavirenz, virus strains harboring one or more of the seven considered resistance mutations have a significant fitness advantage. As a result, these mutations accumulate in the population during the course of therapy (Boucher et al., 1992; Crandall et al., 1999; Molla et al., 1996). When modelling this accumulative evolutionary process we make the following three assumptions:

- (A1) Substitutions do not occur independently. There are preferred evolutionary pathways in which mutations are fixed.
- (A2) The fixation of mutations into the populations is definite, i.e., substitutions are non-reversible.
- (A3) At each time point, the virus population is dominated by a single strain and clones are independent and (possibly erroneous) copies of this genotype.

As mentioned above, previous studies have provided overwhelming evidence for strong dependencies between resistance mutations, as stated in assumption (A1). In fact, the fixation of mutations typically exhibits order constraints that reflect properties of the underlying fitness landscape (Beerenwinkel et al., 2006). For example, if two advantageous mutations show positive epistasis, then they interact synergistically and the double mutation will be fixed more often than expected from the frequencies of the individual substitutions (Michalakis and

Roze, 2004). In other words, the mutations are more likely to occur on the same mutational pathway. On the other hand, if advantageous mutations exhibit negative epistasis, then they interact antagonistically, resulting in mutants that are less fit than expected or even not viable at all. The mutagenetic tree model accounts for lethal mutational patterns by excluding some binary vectors from its state space, which thus encodes only viable mutant types. Mutational patterns in the state space arise from mutation accumulation along one of the pathways specified in the tree and we call these patterns *compatible* with the tree.

Assumption (A2) refers to the non-reversibility of substitutions. It is motivated by the strong selective advantage that each resistance mutation may confer. Due to this strong selective advantage, we interpret the fixation of each resistance mutation as a selective sweep, after which virtually all viable viruses exhibit the mutation. Together with assumption (A1), this implies that resistance mutations accumulate along different pathways by successive sweeps and that both back substitutions and incompatible states result in viruses whose relative fitness is so low that they can be ignored.

The third assumption (A3) ties in with our point of view of a series of selective sweeps. Indeed, immediately after such an incident the population will consist of the new advantageous mutant type and its recent descendants, which are therefore phylogenetically independent. Under this assumption a virus population should exhibit very low genetic diversity. In light of the phylogenetic independence, the aim of our work is different from that of work employing population genetic or phylogenetic methods (Drummond et al., 2002, 2003). Those approaches explicitly model the mutation and selection process and typically aim at inferring global population parameters, such as the global rate of adaptation (Williamson, 2003) or the effective population size (Seo et al., 2002). By contrast, we model the joint probability distribution resulting from this evolutionary process directly, with the goal of inferring individual substitution rates, as the presence of specific mutational patterns determines the therapeutic options of each patient.

The three assumptions discussed above lead us to a hidden Markov model (HMM) whose state space consists of the compatible states of a given mutagenetic tree. We consider unobservable population states and assume a simple error process involving only a false positive and a false negative rate that generates clones from this hidden state. The fixation of each mutation is modeled by an independent Poisson process. Thus, at each time point, we assume the virus population to be dominated by a single mutational pattern and all clonal variation of this unobserved state is modelled as resulting from erroneous copying of this strain.

The remaining part of this paper is organized as follows. In Section 2 we present the data on the seven considered mutations associated with resistance to efavirenz and perform simple permutation tests to assess the validity of assumptions (A2) and (A3). In Section 3, we develop the above outlined mutagenetic tree HMM (mtree-HMM). We present the results from fitting the mtree-HMM to the efavirenz data in Section 4 and conclude in Section 5 where we discuss some of the limitations of our approach.

2. LONGITUDINAL CLONAL HIV SEQUENCE DATA AND MODEL ASSUMPTION

2.1. HIV data. We subsequently analyze a set of longitudinal clonal HIV sequences that have been collected during three clinical studies of efavirenz combination therapy (DMP 266-003, -004, -005). This data set is publicly available at the Stanford HIV drug resistance database (Rhee et al., 2003). Selection of samples, RNA amplification, cloning, and sequencing have

been described in detail by Bachelier et al. (2000) and Bachelier et al. (2001). All patients received the non-nucleoside RT inhibitor efavirenz.

Bachelier et al. (2000) identified a list of amino acid changes in the HIV RT associated with resistance to efavirenz. In particular, they described two alternative pathways to efavirenz resistance, one initiated by mutation K103N (103-pathway), the other by Y188L (188-pathway). In the present data set, for each patient, at most one of these two pathways occurs. We focus here on the 103-pathway, because mutations associated with the 188-pathway were found in only 7 out of 170 patients, which we excluded from further consideration. A total of 3350 clones have been derived from the remaining 163 patients at between 1 and 11 different time points (median = 3, IQR 1–5). From the list of efavirenz resistance mutations associated with the 103-pathway we selected those that occur in at least 2% of clones. This strategy resulted in the seven mutations 103N (frequency 48.1%), 225H (8.0%), 108I (4.9%), 101Q (2.7%), 190S (2.7%), 101E (2.5%), and 100I (2.3%).

As an example for mutational patterns found in the data set, Table 1 shows the clones observed in patient 22, which is also highlighted in Bachelier et al. (2000, Tab. 2) (Viterbi paths such as the one given in Table 1 are discussed in Section 4). This patient is atypical in that before the onset of therapy (week 0), two clones had mutation 103N. In fact, among the 1144 baseline clones only very few already featured the mutations considered here, i.e., mutations 103N (frequency 1.9%), 190S (1.3%), 101Q (0.7%), 101E (0.35%), and 108I (0.08%). Mutations 100I and 225H were not present in any baseline clone. Only six clones (0.52%) harbored a double mutation, namely 103N+190S.

According to Table 1, the first selective sweep, introducing mutation 103N in the virus population of patient 22, has occurred by week 48. By week 70, mutation 225H shows definite signs of manifestation. This behaviour is in support of the assumptions (A2) and (A3) put forward in the Introduction. For a quantitative analysis of these assumptions, we perform randomization tests.

2.2. Statistical tests. Let $N = 163$ be the number of patients in our data set, and let K_{ij} be the number of clones observed in patient $i \in [N] := \{1, \dots, N\}$ at the j -th time point t_{ij} . Moreover, let $y_{ijkm} \in \{0, 1\}$ be the indicator of the presence of mutation $m \in [M] := \{1, \dots, 7\}$ in clone $k \in [K_{ij}]$ derived from patient $i \in [N]$ at time point t_{ij} . We use two test statistics for evaluating the assumptions (A2) and (A3), respectively. In both cases, we treat different patients as independent observations.

The non-reversibility of substitutions (A2) is tested by tracing the change in mutant allele frequency for each patient over time. This frequency is

$$f_{i,j,m} = \frac{1}{K_{ij}} \sum_{k \in K_{ij}} y_{ijkm}, \quad i \in [N], j \in J_i, m \in [M].$$

For each mutation m , our test statistic A_m counts how often its frequency decreases from one time point to the next. Thus,

$$A_m = \frac{1}{N} \sum_{i \in [N]} \frac{1}{J_i - 1} \sum_{j=1}^{J_i-1} I\{f_{i,j,m} > f_{i,j+1,m}\},$$

where I denotes the indicator function. We estimate the distribution of A_m under the null hypothesis of equal probability of increase and decrease of allele frequencies by randomizing the temporal order of the clone populations. Under non-reversibility of substitutions, the

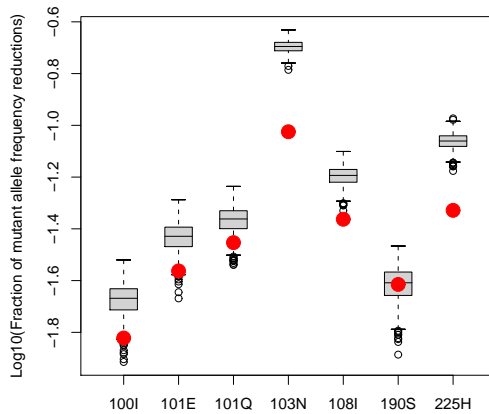


FIGURE 1. Non-reversibility of substitutions. For each mutation, the logarithm of the number of times for which its frequency in the population strictly decreases between successive time points is displayed (bold discs). The distribution of this test statistic was estimated by shuffling 1000 times the order of time points (box plots).

In our data, mutation losses occur in only 1.5 to 9.4% of the cases (Figure 1). In other words, for all seven considered mutations the frequency of the mutant increases or stays constant in over 90% of pairs of subsequent virus populations. For most mutations, this value was significantly smaller than expected ($p_{100I} = 0.011$, $p_{101E} = 0.013$, $p_{103N} < 0.001$, $p_{108I} < 0.001$, $p_{225H} < 0.001$) with the exceptions of mutations 101Q ($p_{101Q} = 0.056$) and 190S ($p_{190S} = 0.465$). We conclude that assumption (A2) of non-reversible substitutions is reasonable for the majority of the data.

For assessing the validity of assumption (A3), we measure the genetic diversity among mutational patterns by the Hamming distance. If c and c' are two clones, their Hamming distance is defined as

$$D_H(c, c') = \sum_{m \in [M]} I\{c_m \neq c'_m\}.$$

The diversity of a population of clones c_1, \dots, c_K is the expected Hamming distance between two clones drawn at random from that population,

$$D_H(c_1, \dots, c_K) = \frac{K(K-1)}{2} \sum_{k < k'} D_H(c_k, c_{k'}).$$

Our test statistic is the expected population diversity

$$B = \frac{1}{N} \sum_{i \in [N]} \frac{1}{J_i} \sum_{j=1}^{J_i} D_H(y_{ij1}, \dots, y_{ijK_{ij}}).$$

We consider the null hypothesis of observing the full diversity present in all clones from one patient at each single time point. The distribution of B under this null is estimated by randomly permuting the assignment of clones to time points. Observed values at the left

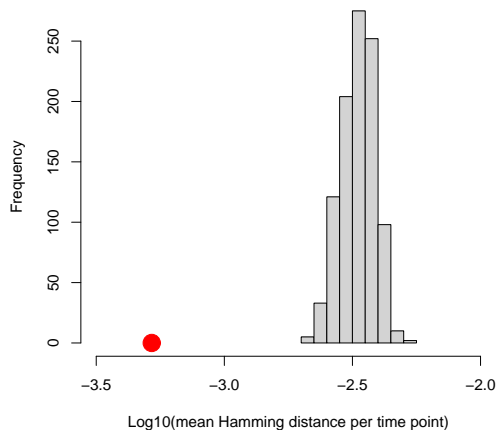


FIGURE 2. Genetic diversity. The logarithm of the average Hamming distance between clones from the same time point is displayed (bold disc). The distribution of this test statistic was estimated by randomizing 1000 times the assignment of clones to time points (histogram).

tail of this distribution indicate less genetic diversity per time point than expected from the total diversity present in the clones. Large population diversities would put into question our assumption of a single population state.

For our data, grouping clones according to their sampling time reduces the genetic diversity more than expected from a random grouping. We find that on average clones from the same population differ in only 1 out of 1900 of the considered mutations (Figure 2). For random clone groupings the expected value is 1 in 300. This difference is highly significant ($p < 0.001$). Thus, most genetic diversity occurs between time points rather than within time points, and most of the observed populations indeed look like having gone through a selective sweep. We therefore conclude that our assumptions described in the Introduction and formalized in the mutagenetic tree HMM, which is described next, are in reasonable agreement with the clonal HIV mutation data considered here.

3. MUTAGENETIC TREE HIDDEN MARKOV MODEL

We begin this section by recalling the basic definition and properties of the mutagenetic tree model for cross-sectional data. We first extend this basic model to a mutagenetic tree Markov chain model for multiple observations per patient in time. Second, we introduce the mutagenetic tree hidden Markov model (mtree-HMM), which assumes the evolutionary state of the virus population to be unobservable. An EM algorithm for parameter estimation is presented, the details of which are given in the Appendix.

3.1. Mutagenetic tree model. Consider M genetic events of interest, which we also call *mutations*. We treat these events as random and use binary random variables to indicate their occurrence. For each mutation $m \in [M] := \{1, \dots, M\}$, let X_m be a binary random variable taking values in $\{0, 1\}$ such that $\{X_m = 1\}$ and $\{X_m = 0\}$ indicate the occurrence and non-occurrence of mutation m , respectively. In the HIV application, $[M]$ represents the

set of seven amino acid changes in the HIV RT described in Section 2 that confer resistance to efavirenz, and X_m indicates the fixation of mutation m into the virus population. For convenience, we additionally introduce a random variable X_0 with $\text{Prob}(X_0 = 1) = 1$. In this setup, the mutational pattern representing the evolutionary state of the virus population corresponds to the binary vector $X = (X_1, \dots, X_M)$ that takes values in the state space $\mathcal{I} = \{0, 1\}^M$.

A *mutagenetic tree* T on M events is a connected branching on the set of vertices $V = \{0\} \cup [M]$, rooted at node 0 (Beerenwinkel et al., 2005b); in the cancer literature, such a tree has been termed *oncogenetic* (Desper et al., 1999; von Heydebreck et al., 2004). In particular, this tree is an acyclic directed graph and thus induces a directed graphical model for the joint distribution of the random vector X (Lauritzen, 1996). The joint distributions for X comprised in this graphical model factor as

$$\text{Prob}(X = x) = \prod_{m \in [M]} \text{Prob}(X_m = x_m \mid X_{\text{pa}(m)} = x_{\text{pa}(m)}),$$

where $x \in \mathcal{I}$, $x_0 := 1$, and $\text{pa}(m) = \text{pa}_T(m)$ denotes the parent of m in T . The *mutagenetic tree model* induced by the tree T is a submodel of the usual graphical model obtained by restricting the conditional probability matrices to the form

$$\vartheta^m = \begin{matrix} & 0 & 1 \\ \begin{matrix} 0 \\ 1 \end{matrix} & \begin{pmatrix} 1 & 0 \\ 1 - \vartheta_{11}^m & \vartheta_{11}^m \end{pmatrix} \end{matrix}$$

where $\vartheta_{ab}^m = \text{Prob}(X_m = b \mid X_{\text{pa}(m)} = a) \in [0, 1]$. The mutagenetic tree model imposes the same conditional independence structure as the graphical model but in addition imposes the constraint that an event can occur only if all of its ancestor events have already occurred (Beerenwinkel and Drton, 2005, Thm. 14.6). This fact follows from the first row of the transition matrix. As a consequence, mutations can only occur in specific pathways. More precisely, each mutational pattern corresponds to a subtree of the mutagenetic tree and the pathways correspond to sequences of subtrees related by inclusion and increasing by exactly one vertex (mutation). The extreme cases are the star and the path. In the star, each vertex has the root vertex as parent and all mutational pathways are possible. In the path, the vertices form a chain starting with the root vertex. In this case, there is only one pathway.

A mutational pattern $x \in \mathcal{I}$ is called *compatible* with the tree T , if x is a state that may occur with non-zero probability in the mutagenetic tree model induced by T . Hence, x is compatible with T , if there exist parameters $\vartheta = (\vartheta_{11}^1, \dots, \vartheta_{11}^M) \in [0, 1]^M$ such that

$$\text{Prob}(X = x) = \prod_{m \in [M]} \vartheta_{x_{\text{pa}(m)}, x_m}^m > 0.$$

The set $\mathcal{C}(T)$ of states that are compatible with the tree T forms a finite distributive lattice $(\mathcal{C}(T), \vee, \wedge)$, where \vee and \wedge denote the component-wise maximum and minimum operator, respectively (Beerenwinkel and Drton, 2005, Lem. 14.3), cf. Figure 3(a),(b). The so-called Hasse diagram in Figure 3(b) illustrates the above-mentioned pathways in that any such pathway corresponds to a path from the (wild-type) state $(0, \dots, 0) \in \mathcal{C}(T)$ to the state $(1, \dots, 1) \in \mathcal{C}(T)$ with all mutations present.

In a *timed mutagenetic tree model*, mutations occur according to independent Poisson processes. If $\lambda_m > 0$ denotes the rate of this process on the edge $\text{pa}(m) \rightarrow m$, then the probability

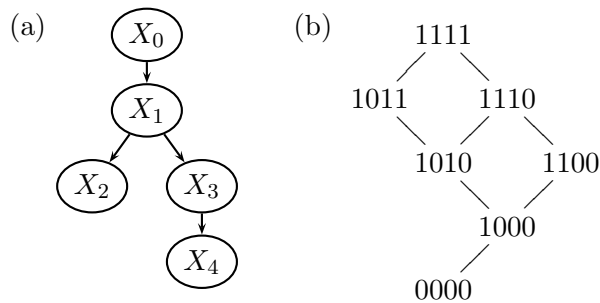


FIGURE 3. (a) Mutagenetic tree on five vertices; and (b) its induced lattice of compatible states.

that mutation m occurs during a time period of length Δt is

$$\vartheta_{11}^m = \text{Prob}(X_m = 1 \mid X_{\text{pa}(m)} = 1) = 1 - e^{-\lambda_m \Delta t}.$$

Mutagenetic trees can be reconstructed from cross-sectional data by solving the maximum weight branching problem in the complete graph on the set of vertices V with an efficient combinatorial algorithm (Desper et al., 1999). This algorithm is implemented, for example, in the `Mtreemix` software package (Beerenwinkel et al., 2005c). Here, we use the algorithm for obtaining the topology (but not the parameters) of the tree. For this purpose, the longitudinal data were treated as cross-sectional.

3.2. Markov chain model. Assume now that we can observe the viral mutational pattern within one patient at more than one time point. More precisely, let X_{jm} be a binary random variable indicating the occurrence of mutation m at time point t_j , $j = 1, \dots, J$, in the patient's virus population. We assume that the evolutionary process starts at time 0 in the wild type state, i.e. without any mutation, which is the case for the majority of our data (cf. Section 2.1). Thus, the initial population state distribution follows the timed mutagenetic tree model. In particular, $X_{1m} = 0$ for all $m \in [M]$ with $t_1 = 0$.

For the temporal evolution of the mutational patterns $X_j = (X_{j1}, \dots, X_{jM})$, $j = 1, \dots, J$, we make the assumption that these vectors form a Markov chain observed at fixed time points $t_1 < t_2 < \dots < t_J$. Furthermore, we assume that a mutation occurs at the time it is observed. In the HIV application, observations can only be made if the virus load is above a detectable limit resulting in censored observations. However, prior work of Foulkes and DeGruttola (2003) suggests that the impact of the censoring is minor (cf. Section 5).

The development of mutation m at a time point t_j with $j \geq 2$ which is encoded in the random variable X_{jm} , depends on past mutational events as well as current ancestral mutational events only through two indicators. The first one is $X_{j-1,m}$ and indicates whether the mutation was already present at the immediately preceding time point t_{j-1} . The second one is $X_{j\text{pa}(m)}$ and indicates whether the parent mutation is present at time point t_j . These dependencies arise from modeling the presence of mutation m at time t_j as resulting either from its introduction along the edge $\text{pa}(m) \rightarrow m$ at time point t_j , or from its earlier non-reversible introduction into the population and hence its presence at time point t_{j-1} . The dependency structure among the variables $(X_{jm} \mid j = 1, \dots, J, m \in [M])$ can be encoded in an acyclic directed graph. For example, the subgraph of the graph shown in Figure 4 induced by the unshaded vertices represents the mutagenetic tree Markov chain based on the tree in Figure 3(a).

The dynamics of this Markov chain model are encoded by the transition matrices

$$(1) \quad \theta_j(\lambda_m) = \begin{matrix} & & 0 & & 1 \\ & 00 & & & 0 \\ & 01 & \left(\begin{array}{cc} 1 & 1 - e^{-\lambda_m(t_j - t_{j-1})} \\ e^{-\lambda_m(t_j - t_{j-1})} & 1 - e^{-\lambda_m(t_j - t_{j-1})} \end{array} \right) & & \\ & 10 & & & * \\ & 11 & & & 1 \end{matrix}$$

whose rows are indexed by pairs $(m, \text{pa}(m))$ in $\{0, 1\}^2$. The asterisks indicate entries that need not be specified, because no event m can occur before its parent event $\text{pa}(m)$. With these matrices we define the *mutagenetic tree Markov chain model* as the family of joint distributions of the form

$$\text{Prob}(X_{jm} = x_{jm}, j = 1, \dots, J, m \in [M]) = \prod_{j=1}^J \prod_{m \in [M]} \theta_j(\lambda_m)_{(x_{j-1,m}, x_{j\text{pa}(m)}), x_{jm}},$$

where $x_{j0} := 1$ and $t_0 := 0$. It follows that

$$\text{Prob}(X_{jm} = x_{jm} \mid X_{j-1,m} = x_{j-1,m}, X_{j\text{pa}(m)} = x_{j\text{pa}(m)}) = \theta_j(\lambda_m)_{(x_{j-1,m}, x_{j\text{pa}(m)}), x_{jm}}.$$

3.3. Mtree-HMM. We now turn to the case of observed clonal samples, rather than population states, at different time points. We model these data by assuming that the clones are erroneous copies of a hidden mutational pattern that evolves according to a mutagenetic tree Markov chain. Hence, X_{jm} is now a hidden binary random variable. The observed data are instances of binary random variables Y_{jkm} , $k \in [K_j]$ that indicate whether mutation m is present in the k -th clone sampled from the virus population at time point t_j . Clones are conditionally independent given the hidden states $(X_j)_{j=1, \dots, J}$. The resulting graphical model is referred to as the *mutagenetic tree hidden Markov model*, or *mtree-HMM* for short. Its graph is shown in Figure 4.

Let $\varepsilon^+ = (\varepsilon_1^+, \dots, \varepsilon_M^+) \in [0, 1]^M$ and $\varepsilon^- = (\varepsilon_1^-, \dots, \varepsilon_M^-) \in [0, 1]^M$ be parameter vectors that contain the mutation-specific probabilities of observing a false positive and a false negative, respectively. False positives (negatives) are mutations (wild type residues) observed in clones derived from a virus population that is in the wild type (mutant) state at that time point. The false positive and false negative rates summarize differences from the population state that can arise from mutations in the PCR reactions, or from erroneous viral copying of the dominating strain. Thus, these parameters quantify the expected genetic diversity of the virus population. Conditionally upon the hidden state X_{jm} , the probabilities of observing mutation m in clone k at time point t_j are

$$\theta'(\varepsilon_m^+, \varepsilon_m^-) = \begin{matrix} & 0 & & 1 \\ & 1 - \varepsilon_m^+ & & \varepsilon_m^+ \\ & \varepsilon_m^- & & 1 - \varepsilon_m^- \end{matrix}.$$

The entries of this matrix are the conditional probabilities

$$\theta'(\varepsilon_m^+, \varepsilon_m^-)_{x_{jm}, y_{jkm}} = \text{Prob}(Y_{jkm} = y_{jkm} \mid X_{jm} = x_{jm}).$$

The different clones $Y_{jk} = (Y_{jk1}, \dots, Y_{jkm})$, $k \in [K_j]$, are thus modeled as independent and identically distributed. Let

$$Y = (Y_{jkm} \mid j = 1, \dots, J, k \in [K_j], m \in [M])$$

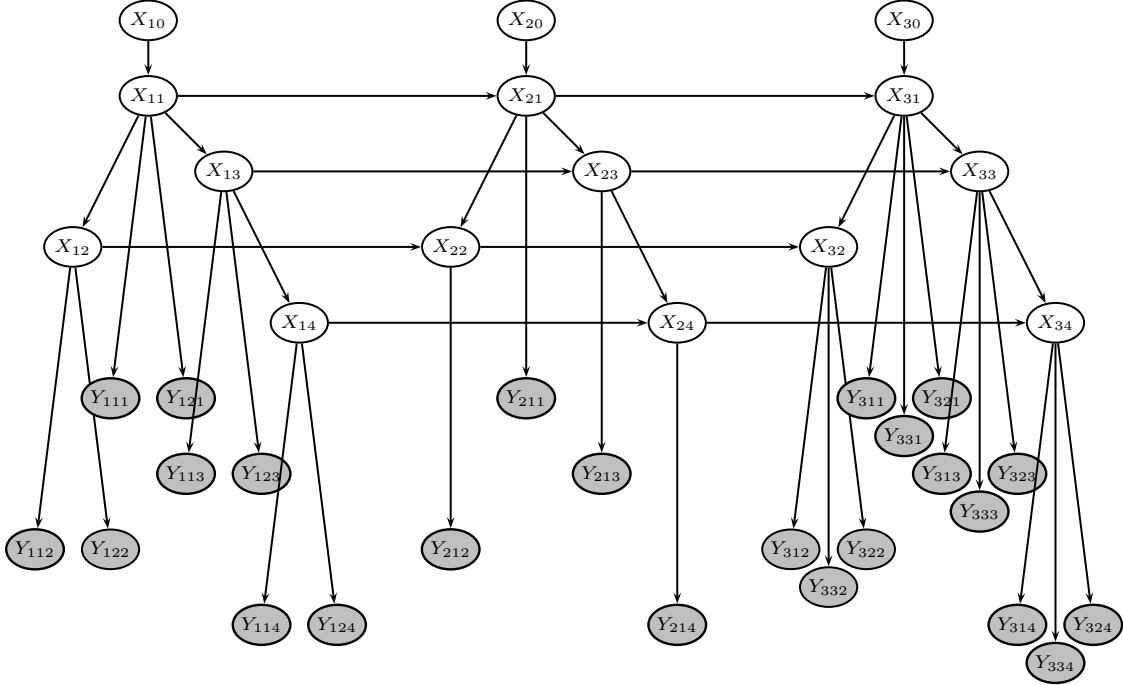


FIGURE 4. Acyclic directed graph representing an mtree-HMM based on the tree from Figure 3(a) with $J = 3$ time points, two clones at time point t_1 , one clone at t_2 , and three clones at t_3 . Clear vertices correspond to hidden random variables, shaded vertices to observable variables.

denote all clonal sequence observations. The *mutagenetic tree hidden Markov model (mtree-HMM)* is the family of joint distributions of Y given by

$$\text{Prob}(Y = y) = \sum_{x_1 \in \mathcal{C}(T)} \cdots \sum_{x_J \in \mathcal{C}(T)} \prod_{m \in [M]} \prod_{j=1}^J \left(\theta_j(\lambda_m)_{(x_{j-1,m}, x_{jpa(m)}, x_{jm})} \prod_{k \in [K_j]} \theta'(\varepsilon_m^+, \varepsilon_m^-)_{x_{jm}, y_{jkm}} \right),$$

where we have summed over the hidden states. The graphical model structure of the mtree-HMM is illustrated in Figure 4.

We remark that on an abstract level mtree-HMMs are related to phylogenetic HMMs (phylo-HMMs) (McAuliffe et al., 2004; Siepel and Haussler, 2004). Phylo-HMMs are probabilistic models of sequence evolution that combine phylogenetic trees at different sites of aligned genomes with an HMM that allows for dependence across sites. Thus, in phylo-HMMs the tree models arise through dependence in time, and the HMM represents a dependence in space (along the genome). While mtree-HMMs are similarly structured in that tree-based models are combined with HMMs, the roles of space and time are reversed. The mutagenetic trees arise from dependence among genome sites, and the HMM introduces dependence across time.

3.4. Parameter estimation. Consider now clonal sequence data for a set of patients indexed by $[N] = \{1, \dots, N\}$. For each patient $i \in [N]$, we have observations at time points $t_{i1} < t_{i2} < \dots < t_{iJ_i}$. We denote by X_{ijm} the indicator of occurrence of mutation m in the viral population state of patient i at time point t_{ij} . The random variable Y_{ijkm} indicates the occurrence of mutation m in clone $k \in [K_{ij}]$ of patient i at time point t_{ij} . We denote the transition matrices (Equation 1) by $\theta_{ij}(\lambda_m)$. For example,

$$\theta_{ij}(\lambda_m)_{01,0} = e^{-\lambda_m(t_{ij}-t_{i,j-1})}.$$

We assume patients to be independent and each patient to follow the mtree-HMM based on a fixed tree T . Then the resulting model for the observations

$$Y = (Y_{ijkv} \mid i \in [N], j = 1, \dots, J_i, k \in [K_{ij}], m \in [M]),$$

made at time points $\{t_{ij} \mid i \in [N], j = 1, \dots, J_i\}$, has the likelihood function

$$L_{\text{obs}}(\lambda, \varepsilon^+, \varepsilon^-) = \sum_{x_{11} \in \mathcal{C}(T)} \dots \sum_{x_{NJ_N} \in \mathcal{C}(T)} \prod_{i \in [N]} \prod_{m \in [M]} \prod_{j=1}^{J_i} \left(\theta_{ij}(\lambda_m)_{(x_{i,j-1,m}, x_{ijpa(m)}, x_{ijm})} \prod_{k \in [K_{ij}]} \theta'(\varepsilon_m^+, \varepsilon_m^-)_{x_{ijm}, y_{ijkm}} \right),$$

where we set $x_{i0m} := 1$ and $t_{i0} := 0$ for all $i \in [N]$ and $m \in [M]$. The outer sums make the likelihood function hard to maximize. In order to solve this optimization problem and to obtain maximum likelihood estimates, we apply an Expectation Maximization (EM) algorithm.

Let $\{x_{ijm}\}$ be values of the hidden variables $\{X_{ijm}\}$ that are compatible with the unobserved mutagenetic tree Markov chain model. Then it must hold that $x_{ijm} = 1$ whenever $x_{i,j-1,m} = 1$ and $x_{ijm} = 0$ whenever $x_{ijpa(m)} = 0$. Let I be the indicator function and set

$$\begin{aligned} \chi_{ijm}(a) &= I\{x_{i,j-1,m} = 0, x_{ijpa(m)} = 1, x_{ijm} = a\}, \\ \chi'_{ijkm}(a, b) &= I\{x_{ijm} = a, y_{ijkm} = b\}, \end{aligned}$$

for $a, b = 0, 1$. The log-likelihood function $\ell_{\text{hid}}(\lambda, \varepsilon^+, \varepsilon^-)$ of the hidden model is the sum over all $i \in [N]$, $m \in [M]$, and $j = 1, \dots, J_i$ of the expressions

$$\begin{aligned} & - \chi_{ijm}(0) \lambda_m (t_{ij} - t_{i,j-1}) + \chi_{ijm}(1) \log(1 - e^{-\lambda_m(t_{ij}-t_{i,j-1})}) \\ & + \sum_{k \in [K_{ij}]} \left[\chi'_{ijkm}(0, 0) \log(1 - \varepsilon_m^+) + \chi'_{ijkm}(0, 1) \log \varepsilon_m^+ \right. \\ & \quad \left. + \chi'_{ijkm}(1, 0) \log \varepsilon_m^- + \chi'_{ijkm}(1, 1) \log(1 - \varepsilon_m^-) \right]. \end{aligned}$$

Maximization of ℓ_{hid} is feasible since it does not involve the sums that are present in L_{obs} .

The EM algorithm iteratively alternates between its E-step, in which the expectations of the indicators χ_{ijm} and χ'_{ijkm} are computed for fixed parameter estimates, and its M-step, in which these expectations are used to maximize the expectation of the log-likelihood function ℓ_{hid} and to obtain new parameter estimates. Details of the EM algorithm, including the choice of starting solutions and the bootstrap procedure for confidence intervals, are given in the Appendix.

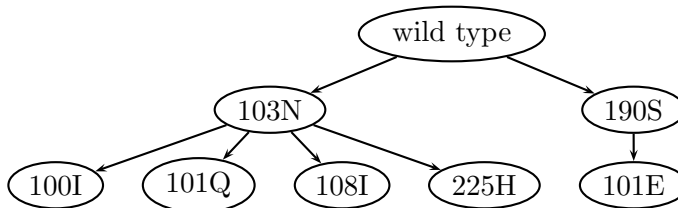


FIGURE 5. Mutagenetic tree model for the development of resistance to efavirenz in the HIV-1 reverse transcriptase. Vertices are labeled with amino acid substitutions.

4. RESULTS

4.1. Tree reconstruction. Employing the cross-sectional tree reconstruction method yielded the mutagenetic tree on 8 vertices displayed in Figure 5 with parameters λ shown in Figure 6(a). In this mutagenetic tree model, predominantly mutation 103N initiates the development of efavirenz resistance and is followed by 100I, 101Q, 108I, or 225H. A parallel but strongly retarded pathway involves mutation 190S followed by 101E. Based on this cross-sectional analysis, the expected waiting time for mutation 103N to occur is estimated to $\hat{\lambda}_{103N}^{-1} = 3.4$ weeks of efavirenz combination therapy. By contrast, mutation 190S is estimated to occur after 113 weeks.

The mutagenetic tree model has 51 compatible states. The transition matrix of the corresponding HMM has 588 nonzero entries out of $51^2 = 2601$ (cf. Appendix).

4.2. Inferred population states. Using the fixed tree topology, we applied the EM algorithm to the longitudinal clonal data. The Viterbi algorithm was used to obtain maximum a posteriori estimates of the hidden variables, i.e. of the viral population states, resulting in one Viterbi path for each patient. Given the model parameters, the Viterbi path is the most probable sequence of states to explain both the progression in time of the virus population along the lattice of compatible states and the observed clones at the respective time points. For example, the Viterbi path for patient 22 is illustrated in Table 1. We estimated mutation 103N to enter the virus population of this patient at week 48 and mutation 225H to be introduced after 70 weeks of therapy. Mutation 103N had already been present in 2 out of 16 clones before onset of therapy (week 0), but was most likely not established in the population at this time, because viral replication was suppressed for 48 more weeks (Bachelier et al., 2000, Fig. 1). Likewise, mutation 225H appears first at week 59 in 1 out of 7 clones, 11 weeks before its estimated fixation. Conversely, we estimated the introduction of this mutation at week 70 despite the fact that 4 out of 8 cloned did not yet harbor it at this time.

4.3. Rates of progression. The parameters λ are conditional rates of fixation of mutations in the population, associated with the edges of the mutagenetic tree. Estimation of these rates from cross-sectional data depends on the assumption of independent observations and of an exponentially distributed sampling time (Equation 2 in the Appendix), both of which are not met with the present data set ($p < 10^{-15}$, Kolmogorov-Smirnov test). Estimates of λ in the mtree-HMM are shown in Figure 6(a).

Mutation 103N is by far the earliest mutation to occur with an expected waiting time of 19 weeks, as compared to 190S with 478 weeks. Subsequent to 103N, mutation 225H is most likely to occur next, followed by 108I, 101Q, and 100I. Mutation 101E appears shortly after 190S.

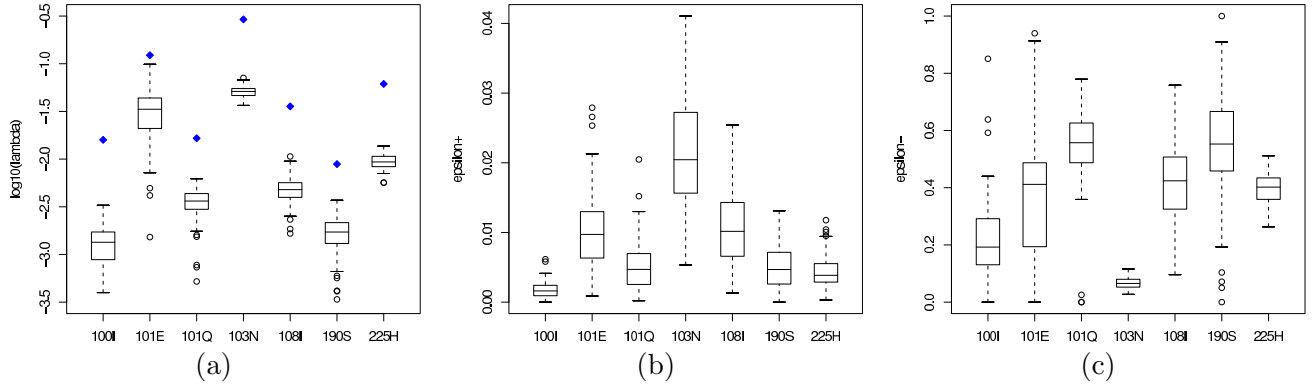


FIGURE 6. Bootstrap estimates of the parameters of the mtree-HMM for the development of efavirenz resistance based on the tree in Figure 5. (a) Progression rates λ of mutations, reported on a log scale. Diamonds indicate the cross-sectional estimate. (b) False positive rates ϵ^+ . (c) False negative rates ϵ^- .

These findings are in accordance with *in vitro* measurements of efavirenz resistance (Bacheler et al., 2001). Engineered single amino acid substitutions result in 36-fold and 97-fold reduced efavirenz susceptibility for 103N and 190S, respectively, as compared to the wild type. By contrast, all other mutations cause significantly less efavirenz resistance on their own (1.2- to 24-fold, median 5.6). Remarkably however, all of the double mutants 103N+100I, 103N+101Q, 103N+108I, 103N+225H as well as the triple mutant 103N+108I+225H were measured highly resistant (84- to 2,400-fold). Thus, phenotypic resistance increases along the mutagenetic tree, and the ordered accumulation appears to result from a specific phenotypic gradient.

Comparing the cross-sectional estimates of λ to their longitudinal counterparts obtained from bootstrapping reveals consistent overestimation of progression rates by the cross-sectional approach (Figure 6(a)). This effect may be due to the high number of clones that have been sequenced prior to therapy start at week 0, which leads to an estimated sampling time of only 22 weeks in the cross-sectional approach.

4.4. Clonal variation. The variation of clones is modeled by mutation-specific parameters ϵ_m^+ and ϵ_m^- that denote the probability of a false positive and a false negative mutation, respectively. Figures 6(b) and 6(c) show the bootstrap estimates of these parameters. False positives occur when a mutation is not yet fixed into the population, but is already present on single clones. We found very low false positive rates (mean < 0.02) for all mutations.

We obtained higher estimates for ϵ^- , the rates of false negatives. False negatives occur when a mutation is estimated to be fixed into the virus population, but does not appear in subsequent clones. This happens more frequently, because the model assumes non-reversibility of mutations in the population. The false negative rate of 103N was by far the lowest, presumably due to its strong selective advantage both as a single mutation and in combination with others. Mutations 190S and 101E showed high false negative rates but these estimates were also subject to a considerable variance. In the case of 190S and also 101Q, the high false negative rate is not as surprising given that the randomization tests in Section 2.2

indicated that the assumption of non-reversibility of substitution is less warranted for these two mutations.

5. LIMITATIONS AND CONCLUSIONS

RNA viruses provide prominent examples of measurably evolving populations, and precise predictions of the outcome of this evolutionary process are a prerequisite for the rational design of antiretroviral treatment protocols. Insight in the evolutionary process can be obtained from longitudinal genomic data. For analysis of such data, we have presented a mutagenetic tree hidden Markov model. We applied this model in an analysis of longitudinal clonal sequence data on the evolution of drug resistance in HIV. Our focus was on estimating the order and rate of occurrence of seven single amino acid changes that are associated with resistance to the drug efavirenz.

Our model of clonal variation assumes that the clones are possibly erroneous copies of a fixed but unobserved population state. Thus, we regard the virus population as consisting of a single dominating strain and a cloud of closely related mutants. While this assumption is justified by the strong selective pressure exerted by antiretroviral therapy, it does not allow for explicit modeling of different lineages following different evolutionary pathways. Such parallel developments were very rare in the present data set. For example, out of the 7 viral clones derived from patient 126 at week 59, 3 clones displayed the mutational pattern 103N-225H, and 5 mutations 190S-101E. The estimated population state was the union of these four mutations, but none of the observed clones actually displayed this pattern. In fact, these parallel lineages contribute to the elevated false negative rates of mutations 101E and 190S. Possible ways of extending the mtree-HMM to account for this effect include modeling the population state as more than one strain, and grouping clones into different pathways.

Evolution in our model is assumed to result from mutation and selection. Incorporating recombination would alter our set-up considerably. However, the mutations we considered lie no more than 125 codons, or 375 nucleotides, apart. Given the HIV genome of length 10,000 base pairs, recombination is unlikely to occur in this small region, but cannot be ruled out entirely.

Finally, we emphasize that throughout we have ignored the interval censoring inherent in the data and assumed that mutations occur at the time they are observed. However, ignoring the interval censoring is unlikely to have a strong effect on the parameter estimates because of the small interval lengths. In a related analysis of data with the same time interval structure, Foulkes and DeGruttola (2003) have found no qualitative and little quantitative difference when using the midpoint of time intervals as the time at which mutations occur. Nevertheless, modeling interval censoring will become more important for larger time intervals, for example due to longer periods of suppressed virus replication below detectable limits.

ACKNOWLEDGMENTS

Niko Beerenwinkel is supported by Deutsche Forschungsgemeinschaft (DFG) under grant No. BE 3217/1-1. Mathias Drton acknowledges support from NIH grant R01-HG02362-03 and NSF grant DMS-0505612.

REFERENCES

- L. Bachelier, S. Jeffrey, G. Hanna, R. D'Aquila, L. Wallace, K. Logue, B. Cordova, K. Hertogs, B. Larder, R. Buckery, D. Baker, K. Gallagher, H. Scarnati, R. Tritch, and C. Rizzo.

- Genotypic correlates of phenotypic resistance to efavirenz in virus isolates from patients failing nonnucleoside reverse transcriptase inhibitor therapy. *J Virol*, 75(11):4999–5008, Jun 2001. URL <http://dx.doi.org/10.1128/JVI.75.11.4999-5008.2001>.
- L. T. Bachelier, E. D. Anton, P. Kudish, D. Baker, J. Bunville, K. Krakowski, L. Bolling, M. Aujay, X. V. Wang, D. Ellis, M. F. Becker, A. L. Lasut, H. J. George, D. R. Spalding, G. Hollis, and K. Abremski. Human immunodeficiency virus type 1 mutations selected in patients failing efavirenz combination therapy. *Antimicrob Agents Chemother*, 44(9):2475–2484, Sep 2000.
- N. Beerenwinkel, M. Däumer, T. Sing, J. Rahnenführer, T. Lengauer, J. Selbig, D. Hoffmann, and R. Kaiser. Estimating HIV evolutionary pathways and the genetic barrier to drug resistance. *J Infect Dis*, 191(11):1953–1960, Jun 2005a. URL <http://dx.doi.org/10.1086/430005>.
- N. Beerenwinkel and M. Drton. Mutagenetic tree models. In L. Pachter and B. Sturmfels, editors, *Algebraic Statistics for Computational Biology*, chapter 14, pages 278–290. Cambridge University Press, Cambridge, UK, 2005.
- N. Beerenwinkel, N. Eriksson, and B. Sturmfels. Evolution on distributive lattices. *submitted*, 2006. URL <http://arxiv.org/abs/q-bio/0511039>.
- N. Beerenwinkel, J. Rahnenführer, M. Däumer, D. Hoffmann, R. Kaiser, J. Selbig, and T. Lengauer. Learning multiple evolutionary pathways from cross-sectional data. *J Comput Biol*, 12(6):584–598, 2005b. URL <http://dx.doi.org/10.1089/cmb.2005.12.584>.
- N. Beerenwinkel, J. Rahnenführer, R. Kaiser, D. Hoffmann, J. Selbig, and T. Lengauer. Mtreemix: a software package for learning and using mixture models of mutagenetic trees. *Bioinformatics*, 21(9):2106–2107, May 2005c. URL <http://dx.doi.org/10.1093/bioinformatics/bti274>.
- N. Beerenwinkel, T. Sing, T. Lengauer, J. Rahnenführer, K. Roomp, I. Savenkov, R. Fischer, D. Hoffmann, J. Selbig, K. Korn, H. Walter, T. Berg, P. Braun, G. Fätkenheuer, M. Oette, J. Rockstroh, B. Kupfer, R. Kaiser, and M. Däumer. Computational methods for the design of effective therapies against drug resistant HIV strains. *Bioinformatics*, 21(21):3943–3950, Sep 2005d. URL <http://dx.doi.org/10.1093/bioinformatics/bti654>.
- C. A. Boucher, E. O’Sullivan, J. W. Mulder, C. Ramautarsing, P. Kellam, G. Darby, J. M. Lange, J. Goudsmit, and B. A. Larder. Ordered appearance of zidovudine resistance mutations during treatment of 18 human immunodeficiency virus-positive subjects. *J Infect Dis*, 165(1):105–110, Jan 1992.
- F. Clavel and A. J. Hance. HIV drug resistance. *N Engl J Med*, 350(10):1023–1035, Mar 2004. URL <http://dx.doi.org/10.1056/NEJM2ra025195>.
- K. A. Crandall, C. R. Kelsey, H. Imamichi, H. C. Lane, and N. P. Salzman. Parallel evolution of drug resistance in HIV: failure of nonsynonymous/synonymous substitution rate ratio to detect selection. *Mol Biol Evol*, 16(3):372–382, Mar 1999.
- R. Desper, F. Jiang, O. P. Kallioniemi, H. Moch, C. H. Papadimitriou, and A. A. Schaffer. Inferring tree models for oncogenesis from comparative genome hybridization data. *J Comput Biol*, 6(1):37–51, 1999.

- A. J. Drummond, G. K. Nicholls, A. G. Rodrigo, and W. Solomon. Estimating mutation parameters, population history and genealogy simultaneously from temporally spaced sequence data. *Genetics*, 161(3):1307–1320, Jul 2002.
- A. J. Drummond, O. G. Pybus, A. Rambaut, R. Forsberg, and A. G. Rodrigo. Measurably evolving populations. *TRENDS Ecol Evol*, 18(9):481–488, Sep 2003.
- R. Durbin, S. Eddy, A. Krogh, and G. Mitchison. *Biological sequence analysis: Probabilistic models of proteins and nucleic acids*. Cambridge University Press, Cambridge, UK, 1998.
- A. Foulkes and V. DeGruttola. Characterizing the progression of viral mutations over time. *J Am Stat Assoc*, 98(464):859–867, 2003.
- M. J. Gonzales, T. D. Wu, J. Taylor, I. Belitskaya, R. Kantor, D. Israelski, S. Chou, A. R. Zolopa, W. J. Fessel, and R. W. Shafer. Extended spectrum of HIV-1 reverse transcriptase mutations in patients receiving multiple nucleoside analog inhibitors. *AIDS*, 17(6):791–799, Apr 2003. URL <http://dx.doi.org/10.1097/01.aids.0000050860.71999.23>.
- I. Hallgrímsson, R. Milowski, and J. Yu. The EM algorithm for hidden Markov models. In L. Pachter and B. Sturmfels, editors, *Algebraic Statistics for Computational Biology*, chapter 12, pages 248–261. Cambridge University Press, Cambridge, UK, 2005.
- S. Lauritzen. *Graphical Models*. Clarendon Press, 1996.
- J. D. McAuliffe, L. Pachter, and M. I. Jordan. Multiple-sequence functional annotation and the generalized hidden Markov phylogeny. *Bioinformatics*, 20(12):1850–1860, Aug 2004. URL <http://dx.doi.org/10.1093/bioinformatics/bth153>.
- Y. Michalakis and D. Roze. Evolution. Epistasis in RNA viruses. *Science*, 306(5701):1492–1493, Nov 2004. URL <http://dx.doi.org/10.1126/science.1106677>.
- A. Molla, M. Korneyeva, Q. Gao, S. Vasavanonda, P. J. Schipper, H. M. Mo, M. Markowitz, T. Chernyavskiy, P. Niu, N. Lyons, A. Hsu, G. R. Granneman, D. D. Ho, C. A. Boucher, J. M. Leonard, D. W. Norbeck, and D. J. Kempf. Ordered accumulation of mutations in HIV protease confers resistance to ritonavir. *Nat Med*, 2(7):760–766, Jul 1996.
- J. Nelder and R. Mead. A simplex method for function minimization. *Computer Journal*, 7:308–313, 1965.
- J. Rahnenführer, N. Beerenwinkel, W. A. Schulz, C. Hartmann, A. von Deimling, B. Wullich, and T. Lengauer. Estimating cancer survival and clinical outcome based on genetic tumor progression scores. *Bioinformatics*, 21(10):2438–2446, May 2005. URL <http://dx.doi.org/10.1093/bioinformatics/bti312>.
- S.-Y. Rhee, M. J. Gonzales, R. Kantor, B. J. Betts, J. Ravela, and R. W. Shafer. Human immunodeficiency virus reverse transcriptase and protease sequence database. *Nucleic Acids Res*, 31(1):298–303, Jan 2003.
- T.-K. Seo, J. L. Thorne, M. Hasegawa, and H. Kishino. Estimation of effective population size of HIV-1 within a host: a pseudomaximum-likelihood approach. *Genetics*, 160(4):1283–1293, Apr 2002.
- R. W. Shafer and J. M. Schapiro. Drug resistance and antiretroviral drug development. *J Antimicrob Chemother*, 55(6):817–820, Jun 2005. URL <http://dx.doi.org/10.1093/>

`jac/dki127`.

- A. Siepel and D. Haussler. Combining phylogenetic and hidden Markov models in biosequence analysis. *J Comput Biol*, 11(2-3):413–428, 2004. URL <http://dx.doi.org/10.1089/1066527041410472>.
- T. Sing, V. Svicher, N. Beerenwinkel, F. Ceccherini-Silberstein, M. D. R. Kaiser, H. Walter, K. Korn, D. Hoffmann, M. Oette, J. K. Rockstroh, G. Fätkenheuer, C.-F. Perno, and T. Lengauer. Characterization of novel HIV drug resistance mutations using clustering, multidimensional scaling, and SVM-based feature ranking. In *9th European Conference on Principles and Practice of Knowledge Discovery in Databases*, 2005.
- A. von Heydebreck, B. Gunawan, and L. Füzesi. Maximum likelihood estimation of oncogenetic tree models. *Biostatistics*, 5(4):545–556, 2004. URL <http://biostatistics.oupjournals.org/cgi/content/abstract/5/4/545?etoc>.
- S. Williamson. Adaptation in the env gene of HIV-1 and evolutionary theories of disease progression. *Mol Biol Evol*, 20(8):1318–1325, Aug 2003. URL <http://dx.doi.org/10.1093/molbev/msg144>.

APPENDIX A. EXPECTATION MAXIMIZATION ALGORITHM

We provide here a detailed description of the EM algorithm from Section 3.4 that is used to estimate the parameters of the mtree-HMM.

A.1. M-step. The log-likelihood function ℓ_{hid} of the hidden model decomposes into a sum involving only λ and another sum involving only ε^+ and ε^- . Let

$$u_{ijm,a} = \text{Prob}(x_{i,j-1,m} = 0, x_{ijpa(m)} = 1, x_{ijm} = a \mid Y),$$

be the conditional expectation of $\chi_{ijm}(a)$ given the clonal observations Y . For maximum likelihood estimation of λ , we have to maximize the function

$$\sum_{i \in [N]} \sum_{m \in [M]} \sum_{j=1}^{J_i} \left[-u_{ijm,0} \lambda_m (t_{ij} - t_{i,j-1}) + u_{ijm,1} \log(1 - e^{\lambda_m (t_{ij} - t_{i,j-1})}) \right].$$

This task is complicated by the log terms, but can be accomplished numerically by simple general optimization methods, such as the simplex method of Nelder and Mead (1965).

For estimating ε^+ and ε^- let

$$u'_{m,ab} = \sum_{i \in [N]} \sum_{j=1}^{J_i} \sum_{k \in [K_{ij}]} \text{Pr}(x_{ijm} = a, y_{ijkm} = b \mid Y)$$

be the conditional expectation of the corresponding sum of $\chi'_{ijkm}(a, b)$ given the clonal observations Y . Then the maximum likelihood estimates are

$$\hat{\varepsilon}_m^+ = \frac{u'_{m,01}}{u'_{m,00} + u'_{m,01}}, \quad \hat{\varepsilon}_m^- = \frac{u'_{m,10}}{u'_{m,10} + u'_{m,11}}, \quad m \in [M].$$

A.2. E-step. The mtree-HMM is a submodel of a standard HMM with hidden state space equal to the set $\mathcal{C}(T)$ of states compatible with the mutagenetic tree T . Therefore, we can compute the conditional expectations $u_{ijv,a}$ and $u'_{m,ab}$ by applying, separately for each patient, the forward-backward equations of the standard HMM (Durbin et al., 1998; Hallgrímsson et al., 2005). In the standard HMM only certain transitions between compatible states can occur with non-zero probability, namely those that respect the partial order " \succeq " of the lattice induced by T . The probability $\text{Prob}(X_{ij} = \bar{x} \mid X_{i,j-1} = x)$ of transitioning from state $x \in \mathcal{C}(T)$ to state $\bar{x} \in \mathcal{C}(T)$ is given by

$$\prod_{m \in [M]} \theta_{ij}(\lambda_m)_{(x_m, \bar{x}_{\text{pa}(m)}, \bar{x}_m)} = \begin{cases} \frac{\text{Prob}(W=\bar{x})}{\zeta} & \text{if } \bar{x} \succeq x, \\ 0 & \text{else,} \end{cases}$$

where $\zeta = \sum_{x' \succeq x} \text{Prob}(W = x')$ and $W \in \mathcal{I}$ is a random vector distributed according to the timed mutagenetic tree model based on the tree T and the time interval $\Delta t = t_{ij} - t_{i,j-1}$. The number of compatible states depends on the topology of T but is bounded by $M+1 \leq |\mathcal{C}(T)| \leq 2^M$. Thus the number of non-zero transition probabilities also depends on the topology of T . For example, the transition matrix arising from the tree T shown in Figure 3(a) is of the form

$$\begin{array}{c} \begin{matrix} & 0000 & 1000 & 1010 & 1100 & 1011 & 1110 & 1111 \end{matrix} \\ \begin{matrix} 0000 \\ 1000 \\ 1010 \\ 1100 \\ 1011 \\ 1110 \\ 1111 \end{matrix} \begin{pmatrix} * & * & * & * & * & * & * \\ 0 & * & * & * & * & * & * \\ 0 & 0 & * & 0 & * & * & * \\ 0 & 0 & 0 & * & 0 & * & * \\ 0 & 0 & 0 & 0 & * & 0 & * \\ 0 & 0 & 0 & 0 & 0 & * & * \\ 0 & 0 & 0 & 0 & 0 & 0 & * \end{pmatrix}, \end{array}$$

where asterisks indicate entries that are not restricted to zero.

The remaining structure of the standard HMM is determined by the probability of emitting clones $y_{ij1}, \dots, y_{ijK_{ij}}$ from a hidden state $x \in \mathcal{C}(T)$, which is equal to

$$\prod_{m \in [M]} \prod_{k \in [K_{ij}]} \theta'(\varepsilon_m^+, \varepsilon_m^-)_{x_m, y_{ijkm}}.$$

Applying the forward-backward equations to this HMM yields, for each patient i and time point t_{ij} , the conditional expectation of the number of transitions $U_{ij,x\bar{x}}$ from state $x \in \mathcal{C}(T)$ to state $\bar{x} \in \mathcal{C}(T)$, and the conditional expectation of the number of emissions $U'_{ij,xy}$ of clone $y \in \mathcal{I}$ from state $x \in \mathcal{C}(T)$. From these conditional expectations, we can obtain the quantities

$$u_{ijm,a} = \sum_{\substack{\{(x,\bar{x}) \in \mathcal{C}(T) \times \mathcal{C}(T) : \\ x_m=0, \bar{x}_{\text{pa}(m)}=1, \bar{x}_m=a\}}} U_{ij,x\bar{x}},$$

$$u'_{m,ab} = \sum_{i \in [N]} \sum_{m \in [M]} \sum_{j=1}^{J_i} \sum_{\substack{\{(x,y) \in \mathcal{C}(T) \times \mathcal{I} : \\ x_m=a, y_m=b\}}} U'_{ij,xy}$$

that are needed in the M-step of the EM algorithm for the mtree-HMM.

If several vertices of the mutagenetic tree share the root vertex 0 as parent, additional computational saving is possible by employing that variables in different subtrees rooted at 0

are mutually independent. In this case several standard HMMs with smaller state spaces can replace the one standard HMM.

A.3. Starting solutions. As initial parameter values in the mtree-HMM we used 0.1 for all error probabilities ε_m^+ and ε_m^- . The initial rates λ were derived from the cross-sectional approach by assuming an exponential distribution with rate λ_T for the sampling times. Under this assumption λ can be computed from

$$(2) \quad \vartheta_{11}^m = \frac{\lambda_m}{\lambda_m + \lambda_T}, \quad m \in [M],$$

where both ϑ_{11}^m and λ_T were estimated directly from the cross-sectional data (Rahnenführer et al., 2005).

A.4. Confidence intervals. We obtained confidence intervals for all model parameters λ , ε^+ , and ε^- from 100 bootstrap runs of the EM algorithm. Resampling of the data was performed in two steps. First, a set of 163 patients was drawn at random. Second, for each patient and each time point, the corresponding set of clones was used for resampling the respective number of clones. Thus, the number of patients, the structure of sampling times, and the number of clones equaled those of the original data set in all bootstrap runs.

DEPT. OF MATHEMATICS, UNIVERSITY OF CALIFORNIA, 1073 EVANS HALL, BERKELEY, CA 94720
E-mail address: niko@math.berkeley.edu

DEPT. OF STATISTICS, THE UNIVERSITY OF CHICAGO, 5734 S. UNIVERSITY AVE., CHICAGO, IL 60637
E-mail address: drton@galton.uchicago.edu